JOURNAL OF Materials CHEMISTRY

# Water-assisted reconstruction on ferroelectric domain ends of triglycine sulfate $(NH_2CH_2COOH)_3{\cdot}H_2SO_4$ crystals

**Subramanian Balakumar and Hua C. Zeng***

*Department of Chemical and Environmental Engineering, Faculty of Engineering, National University of Singapore, 10 Kent Ridge Crescent, Singapore 119260*

***Received 4th October 1999, Accepted 8th December 1999***

With a humidity-controlled AFM system, water-assisted reconstruction of triglycine sulfate (TGS) crystal surfaces has been investigated for two 180° ferroelectric domains. At high humidity, both holes and islands are found on the two different domain ends, owing to a strong dissolution of the TGS. The island growth on a negative domain end is accompanied by a simultaneous hole-enlargement. When humidity is lowered for a negative domain, the holes are filled up and the islands are increased and linked together at the same time. After a longer reconstruction time at the same low humidity, the islands on the negative domain reduce their sizes, owing to water-assisted molecular relocations. For a positive domain at high humidity, tiny holes can be formed inside an island. However, the hole-number in a positive domain decreases significantly when humidity is reduced. The driving force for surface reconstruction can be associated with the molecular and crystal structures, surface mass transport, and minimization of total energy. Based on the surface topographies investigated at low humidity, the domain polarity of the TGS crystal can be assigned unambiguously.

## Introduction

Triglycine sulfate (TGS, $(NH_2CH_2COOH)_3{\cdot}H_2SO_4$) is one of the well-studied ferroelectric materials.[1–4] Recent research interest in both pure and doped TGS crystals has increased because of the promise of the material for various ferroelectric applications.[3] Much effort in material synthesis has been made to improve the ferroelectric properties of TGS by doping amino acids and phosphate into its single crystals, and fundamental investigations are in rapid progress.[5–8]

TGS is ferroelectric at room temperature and exhibits spontaneous polarization ($P_s$) along *b*-axis ($\langle 010 \rangle$ directions) of the crystal.[1–3] It shows a typical second order ferroelectric phase transition at the Curie point $T_c = 49\,^{\circ}C$. Above the Curie temperature, the structure gains an additional set of mirror planes in the space group $P2_1/m$. Below the Curie point, spontaneous polarization $P_s$ arises along the *b*-axis and it belongs in the polar space group $P2_1$ of the monoclinic crystal system ($a = 0.9417$ nm, $b = 1.2643$ nm, $c = 0.5735$ nm, $\beta = 110^{\circ}\,23'$).[1–4] The crystal, however, splits into an *almost* equal number of positive and negative domains. In other words, antiparallel domains (or 180° domains) along two *b*-directions are formed due to the spontaneous polarization generated at $T < T_c$.[1–4]

In material characterization, the structure and morphology of the TGS family of crystals have been well studied at microscopic and semi-microscopic levels using both optical and electron microscopy techniques.[4,9] Unlike ceramic ferroelectrics,[10–13] which are insoluble in water, TGS is hygroscopic in nature.[4,9,14] Many studies on TGS are based on its hygroscopic nature. For example, using deionized water as a "chemical" etchant, etching studies with SEM have been carried out in order to find defects and domain configuration on a cleaved (010) surface.[4,9] Nonetheless, the SEM technique is unable to investigate surface dynamics and reconstruction, due to difficulties in sample preparation and low vertical resolution. With the advance of the atomic force microscope (AFM), etching patterns and domain structures on the (010) surface of TGS with two different polarities have been studied tridimensionally in greater detail. Much work using the AFM has been reported.[14–24] In particular, high-resolution domain structure, surface charge distribution, surface frictional forces, and domain dynamics at defined temperatures have been investigated. Although it has been proposed that surface topography of TGS is related to a dissolution and recrystallization process,[15,16] detailed information on this reconstruction process is still largely unknown, especially the influence of water (vapor) concentration in the atmosphere above the crystal surface (*i.e.*, humidity) from which water molecules can be condensed into a thin liquid film.[15,16,21] Correlation between the humidity and surface structural reconstruction is not available at this time.

In synthetic chemistry, TGS can be formed by reaction (1):

$$3NH_2CH_2COOH + H_2SO_4 \rightarrow (NH_2CH_2COOH)_3{\cdot}H_2SO_4 \quad (1)$$

The chemical formula $(NH_2CH_2COOH)_3{\cdot}H_2SO_4$ for TGS is rather complicated and numerous molecular groups are present in the unit cell of the substance, as shown in Fig. 1.[1–3] At the molecular level, solid state TGS can be viewed as comprising chemical entities of $2(N^+H_3CH_2COOH)$ (denoted as G1 and

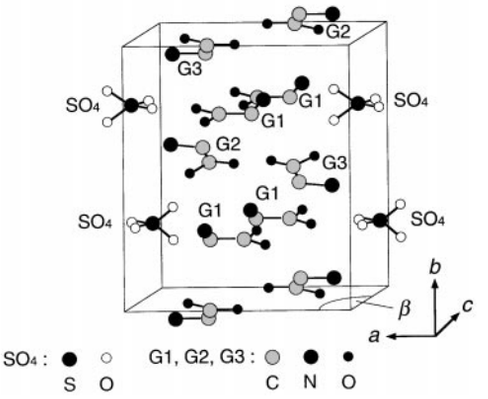


**Fig. 1** Crystal structure of triglycine sulfate (TGS). Along the *b*-axis, the G1–$SO_4$ and G2–G3 layers are stacked alternately. The nearest two neighboring layers with identical chemical composition are rotated 180° around the *b*-axis against each other. Hydrogen atoms are not shown.

G2), $N^+H_3CH_2COO^-$ (denoted as G3) and $SO_4^{2-}$ (Fig. 1).[25,26] Through various intermolecular and intramolecular hydrogen bonds, the molecular species are held together.[1–3,25,26] When exposed to polar water molecules, the solid state hydrogen bonds will be broken and replaced by water-coordinated hydrogen bonds (*i.e.*, hydrated ionic species) when a thin film of liquid water is condensed onto the crystal surface. As a result, TGS molecules of the crystal will then dissolve into the aqueous phase. Recently, we have studied domain boundary motion under a fixed humidity and have determined some critical humidity for the (010) plane dissolution and recrystallization.[14,27] In this paper, we will present a first-time AFM observation on water-assisted surface dynamics reconstruction for two different domains (positive and negative) of TGS at variable humidity. The present work looks into the chemical and material issues of hole and island formation and elimination, local mass transfer, long range mass relocation, and molecular mobility of TGS on the two ferroelectric domain ends. Related to its material chemistry, molecular behaviors of TGS on the two different domain ends are vastly different. Based on humidity-controlled surface topography, as obtained in this work, polarity of a TGS domain can be determined unambiguously *via* AFM.

## Experimental

Single crystals of pure TGS (fully transparent and colourless) used in this work were grown in aqueous solutions of TGS below the Curie point (49 °C) by a slow cooling method, as detailed in the literature.[4–6] Water-assisted surface reconstruction of the (010) crystal plane of TGS was studied using a WET-SPM system (Shimadzu, SPM-9500) which includes an AFM inside a humidity-controlled chamber. The (010) sample plates were prepared by cleaving a long bar of *b*-cut as-grown single crystal of TGS with a razor blade at room temperature under ambient conditions, and then loaded into the AFM chamber.

The AFM apparatus was operated in the contact mode. An insulating $Si_3N_4$ tip cantilever with a spring constant of about $0.12\ N\ m^{-1}$ was used for the surface topography measurements. Two sets of AFM experiments were conducted respectively under normal ambient conditions and controlled humidity and temperature conditions. When the chamber was opened, the AFM measurements were carried out under normal ambient conditions (*i.e.*, laboratory conditions: relative humidity (RH) = 70% and 26 °C). When the chamber was closed, humidification of background ambience was attained by using a stream of purified air and a commercial auto-humidifier (Shimaden SR-35) operated with a water steam bath at set temperatures. The humidified air of definite RH or dry purified air was sent to the AFM chamber constantly at normal atmospheric pressure (1 atm). The humidity and temperature of the chamber atmosphere were monitored respectively with a humidity-meter and a thermal couple situated inside the chamber. Finally, it should be mentioned that even under high humidity conditions, the charge effect of the $Si_3N_4$ tip can be ignored, since the TGS crystal was grown from a saturated solution which was acidic (eqn. (1)) and close to the isoelectric point of the tip at around pH = 5.

## Results

### Formations of islands and holes on a (010) surface

When a TGS crystal is cleaved along the (010) plane, holes and islands on this surface are often observed.[14–24] These observed surface morphologies have been broadly related to directions of spontaneous polarization of ferroelectric domains.[14–24] For example, hole formation is assigned mainly to the positive domain end while round islands (or terraces) are assigned to the negative domain.[14,15,17–19]

In fact, surface topography of the TGS crystal is very complex, as it also relies heavily on experimental conditions. Since TGS molecules on the surface are bonding-unsaturated, water molecules from the vapor phase will be adsorbed or condensed onto the surface, resulting in formation of a thin liquid film.[15,16] Without defining humidity and temperature, it is easy to cause confusion for domain polarity assignment. This will be demonstrated in Fig. 2(a) for a negative domain and Fig. 2(b) for a positive domain.

Figs. 2(a) and 3(a) display the surface topography of a (010) cleaved plane of TGS after 2 h exposure to ambient conditions (RH = 70% and 26 °C). Both islands (light color with circular shapes) and holes (dark dots) are formed simultaneously on the surface; it should be noted that the lateral dimension of the holes is much smaller than that of the islands. The depth of holes and the height of islands measured from line profiles are a half of the lattice constant of the unit cell along the *b*-axis ($b/2 = 0.7 \pm 0.1$ nm).[14–24] Figs. 2(b) and 3(b) show another cleaved (010) surface of TGS after 1 h under the same ambient conditions (at RH = 70% and 26 °C). Again, both islands and holes can be observed on the same surface, although the island density is lower and more irregular in this case. The depth and height of these holes and islands are the same as those in Fig. 2(a).[14–24]

Apart from the similarities shown in Figs. 2(a) and 2(b), there are also distinct differences between the above two cases. First, small holes are formed inside the islands (Fig. 2(b)) whereas no such holes are observed in the former case (Fig. 2(a)). Second, there are holes formed immediately next

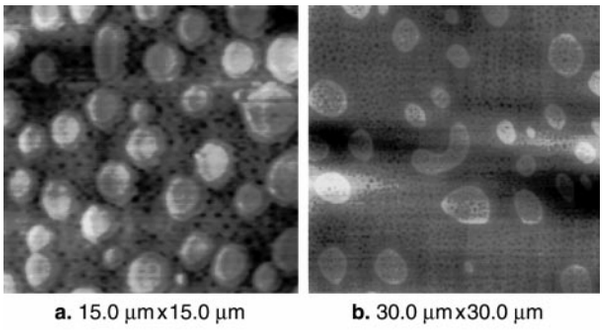


**Fig. 2** AFM micrographs of two cleaved (010) surfaces of TGS crystal with two different surface topographies: (a) a negative domain imaged at 2 h after cleavage of the crystal (RH = 70% and 26 °C), and (b) a positive domain imaged at 1 h after cleavage of the crystal (RH = 70% and 26 °C).

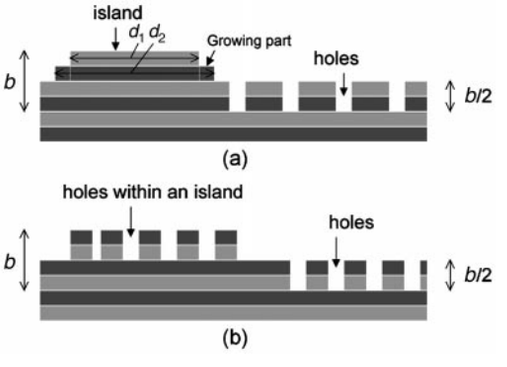


**Fig. 3** Schematic illustrations for the two surface topographies observed in Fig. 2: (a) islands and holes formed in a negative domain end ($d_1$ and $d_2$ are island diameters in the first layer and the second layer respectively), and (b) holes and islands formed in a positive domain end. Light grey layers represent a G2–G3 arrangement while dark grey layers are G1–$SO_4$.

to the flat islands (Fig. 2(a)) whereas there are no such holes in the areas around the irregular islands (Fig. 2(b)).

Based on the above observations at high humidity alone, it is difficult to assign the domain polarity for the two plane topographies. If one considers solubility differences between the two 180° domains,[28] however, the former case seems to be "negative" and the latter "positive".[14–24] These preliminary assignments will be further confirmed below.

### Evolution of islands and holes on negative domain end

For a negative domain, it has been found that the topmost terminal layer of the (010) plane is in a G2–G3 molecular arrangement.[14–24] Islands formed on this domain end have a G2–G3 then a $SO_4$–G1 stacking sequence along the *b*-axis (see both Fig. 1 and Fig. 3).

It should be noted that the round island cliffs on the negative end shown in Fig. 2(a) are not abrupt. In fact, the second layer in the islands is larger than the first, *i.e.*, $d_1 < d_2$ (Fig. 3(a)), under these high humidity conditions. A cross-sectional depth profile reveals that the difference in the island edge has a vertical distance of *b*/4, as illustrated in Fig. 3(a).

With a longer time at this humidity and temperature, the topography of Fig. 2(a) shows some pronounced changes. Primarily, two changes have been observed with time. In Fig. 4, the diameter of the second layer increases with time while that of the topmost layer remains unchanged. In other words, the dimension $d_2$ is growing in all directions whereas there is no obvious growth in $d_1$ (Fig. 3(a)). In association with this growth, the holes are being enlarged with time at this humidity (RH = 70%). It should be mentioned that, in accordance with the hole-enlargement, the crystal surfaces of Fig. 4(c) and 4(d) are less even, especially in the hole area. To exclude a possible contribution from the $Si_3N_4$ tip, surface areas other than the one in Fig. 4 (the sample area in Fig. 4 was scanned several times) have also been scanned. Topographies of the freshly scanned areas are identical to those in Fig. 4. Therefore the possibility of tip-induced reconstruction can be ruled out.

When the humidity is reduced from 70% to 51%, the second layer growth is shown in Fig. 5 ((a) to (b)). The growth of the topmost layer can also be observed. With this island growth, in

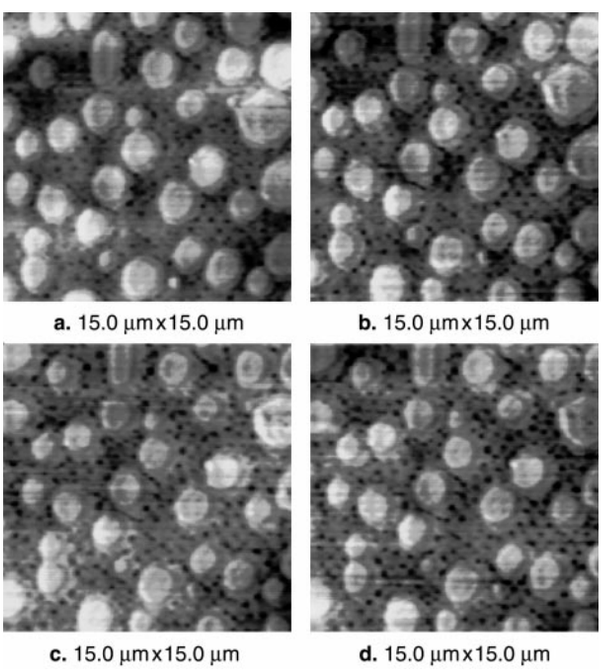


**Fig. 4** Surface reconstruction in a negative domain at constant humidity and temperature (continued from Fig. 2(a), RH = 70% and 26 °C) at (a) 3 h, (b) 4 h, (c) 5 h, and (d) 6 h after the cleavage. Average hole sizes: (a) 0.25 μm, (b) 0.28 μm, (b) 0.31 μm, and (c) 0.33 μm.

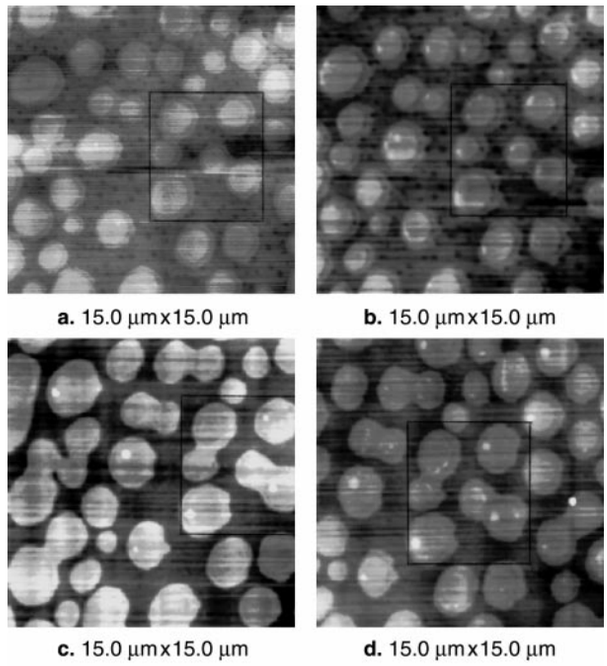


**Fig. 5** Dehumidification and surface reconstruction in a negative domain at (a) 7 h (continued from Fig. 4, RH = 70% and 26 °C), (b) 9 h (RH = 50–52% and 26 °C), (c) 24 h (RH = 50–52% and 26 °C), and (d) 26 h (RH = 50–52% and 26 °C) after the cleavage.

both the topmost and the second layers, some separate islands are now joined together, as shown in Fig. 5(c) for the case of prolonged growth. Pair-joining (two round islands to form an oval island) is a typical merger fashion. Surprisingly, the holes are filled up during the dehumidification, even though the island growth continues. Furthermore, tiny islands (white spots in (c) and (d) of Fig. 5) are formed on top of the original islands and enlarge with time ((c) to (d) in Fig. 5), whose height along the *b*-axis is also *b*/2, based on the AFM cross-sectional data.

With prolonged standing at this low humidity (RH = 51%), as shown in Fig. 6, some of the paired and/or round islands merge together to form irregular islands (the wavy-shaped islands on the right-hand side of (b) to (d) of Fig. 6). It is clear that the small isolated islands are vanishing at a much faster rate than the large islands (see the two dashed frames in (c) and (d)). The total island-density is reduced significantly as indicated by the total island area.

By this time (Fig. 6(c) and 6(d)), the (010) crystal surface of TGS shows only islands (and absolutely no holes) after sequential reduction in humidity and surface reconstruction (Figs. 2(a), 3(a), 4, 5, and 6). According to the AFM results,[14–24] the crystal termination with only island topography can now be assigned unambiguously to a negative domain end.

### Evolution of holes and islands on positive domain end

In contrast to the negative domain, the topmost terminal layer of a positive domain on the (010) surface is in a $SO_4$–G1 molecular arrangement.[23,24] Holes (and islands, if any) formed on this domain end have a $SO_4$–G1 then a G2–G3 stacking sequence along the *b*-axis (see both Fig. 1 and Fig. 3).

For the crystal surface of a positive domain end shown in Fig. 2(b), both holes and islands are observed. However, the number of holes is decreased significantly upon a sequential dehumidification from RH = 70% to 54%, as indicated in Fig. 7. Combination of small holes leads to the formation of larger holes. Reduction in island size is also observed for the islands that contain holes. For example, the island marked with a frame in Fig. 7(a) has 3 holes. The hole-number reduces to 2, 1 and 0 respectively in the images of (b) to (d) over a 6 h period.

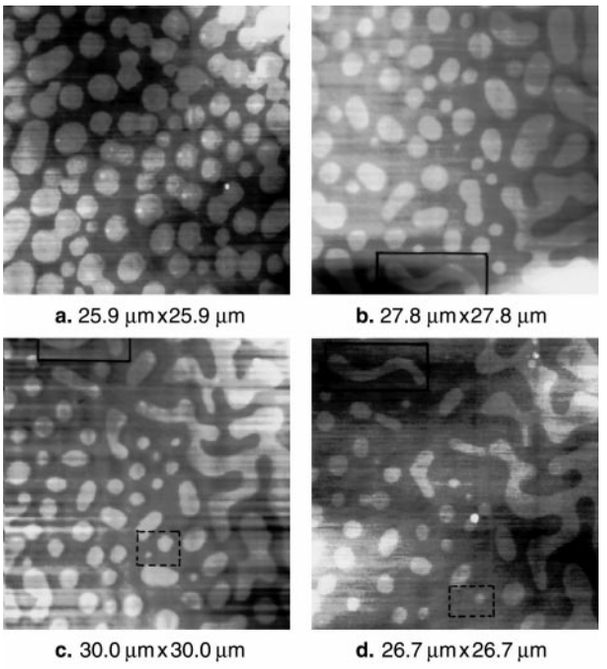


**Fig. 6** Surface reconstruction in a negative domain at constant low humidity (continued from Fig. 5, RH = 50–52% and 26 °C) at (a) 28 h, (b) 70 h, (c) 75 h, and (d) 101 h after the cleavage. A wave-like island is framed (with solid lines) in (c) to (d) to indicate its relative position among the islands. Two dashed line frames in (c) and (d) indicate the process of island size reduction.

For isolated hole-free islands, in contrast, the size is fixed throughout the course of the experiment.

In Fig. 8, a set of AFM images is displayed for the same surface as that of Fig. 7 but at constant RH = 54% and 26–32 h after the crystal cleavage. Compared to those in Fig. 7, the holes in Fig. 8 have expanded significantly while the islands keep about the same sizes. Using the framed area as a reference,

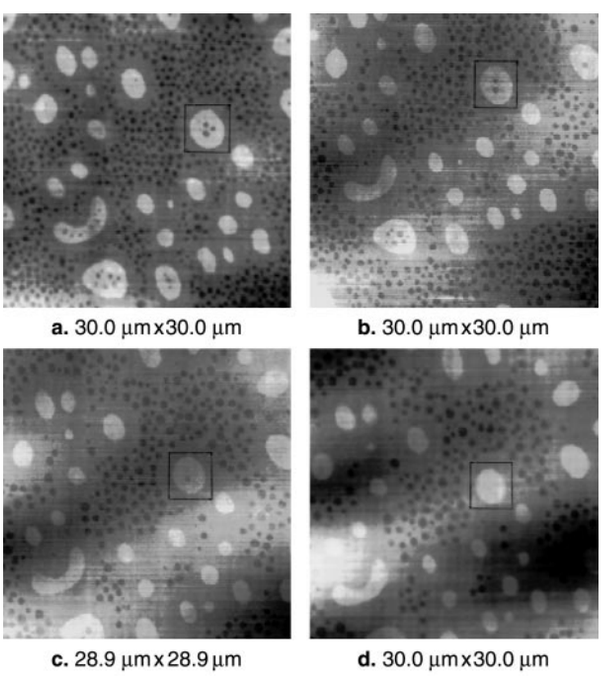


**Fig. 7** Dehumidification and surface reconstruction in a positive domain at (a) 2 h (continued from Fig. 2(b), RH = 57% and 26 °C), (b) 3 h (RH = 56% and 27 °C), (c) 5 h (RH = 54% and 27 °C), and (d) 8 h (RH = 54% and 27 °C) after the cleavage.

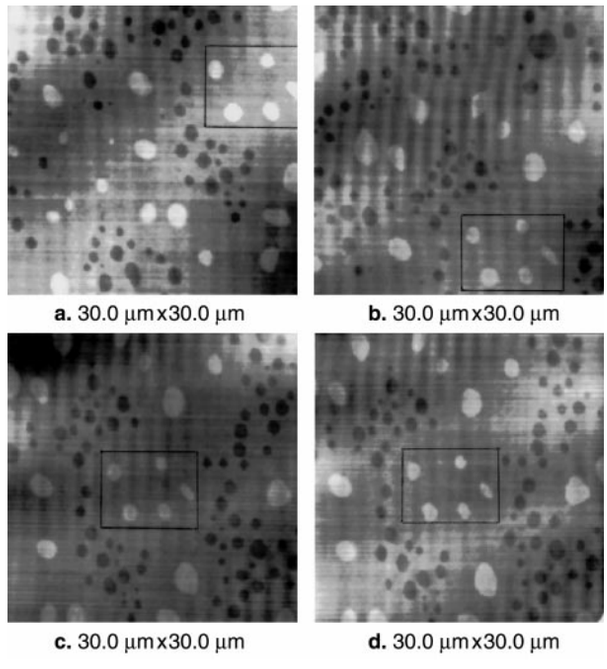


**Fig. 8** Surface reconstruction in a positive domain at constant low humidity (continued from Fig. 7, RH = 54% and 27 °C) at (a) 26 h, (b) 27 h, (c) 30 h, and (d) 32 h after the cleavage.

it is found that there are almost no noticeable changes over the 6 h examination period. In other words, the crystal topography shown in Fig. 8 represents an equilibrium state of the surface under these experimental conditions.

In contrast to the surface reconstruction for the negative domain end (Fig. 5), in which the holes can be eliminated upon dehumidification, the holes shown in Fig. 8 cannot be filled up under similar conditions. Apparently, this crystal topography represents another type of surface termination, positive domain end, in view of the persistence of the hole formation on this surface.[14–24]

## Discussion

### Growth of second layer of islands on a negative domain

On a negative domain end, the topmost layer contains only glycine molecules in two different forms (G2 and G3).[14,15,17–19] Based on the structural data,[1–3,25,26] it is known that the G2 plays the role of glycinium ion $N^+H_3CH_2COOH$ while G3 behaves as a "zwitterion" $N^+H_3CH_2COO^-$ (eqns. (2), (3)).

$$NH_2CH_2COOH + H^+ (\text{from } H_2SO_4) \rightarrow N^+H_3CH_2COOH \quad (2)$$

$$NH_2CH_2COOH \rightarrow N^+H_3CH_2COO^- \quad (3)$$

Since the glycinium ion carries a positive charge and the "zwitterion" is nominally neutral as a whole, the growth of the topmost layer alone is not possible due to the "positive" to "positive" ionic repulsion. On the other hand, the second layer contains both positive glycinium ion ($G1^+$) and negative sulfate ions ($SO_4^{2-}$). It is thus recognized that the growth for an island on a negative domain end must start from the second layer due to the presence of two oppositely charged species. Growth of the second layer is indeed observed for the first time in the present work. As shown in Fig 4, the second layer grows faster than the first at high humidity, *i.e.*, $d_2 > d_1$ ($d_1$ is almost a constant). It should be noted that the extending second layer carries extra negative charges ($\delta-$). These extra negative charges can be partially balanced by the low-dimensioned topmost layer [$(1-x)\delta+$] and partially by the third layer below ($x\delta+$) that also has the G2–G3 structure, as explained in

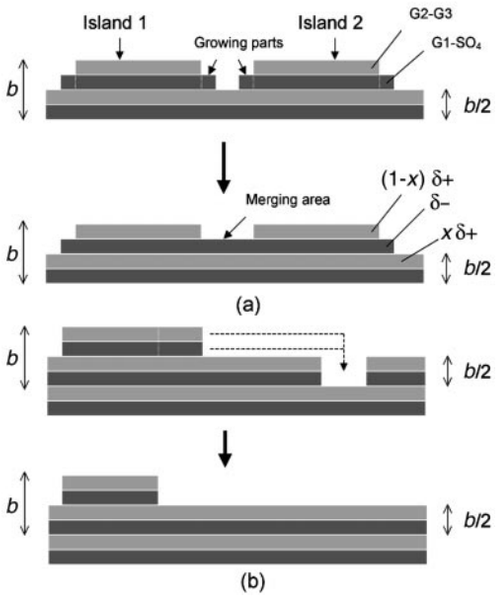


**Fig. 9** Schematic illustrations of restructuring mechanisms: (a) the second layer growth and charge compensation at high humidity. Total negative charge $\delta-$ in the second layer is balanced by the $x\delta+$ in the third layer and $(1-x)\delta+$ in the first layer noting that $x\delta+(1-x)\delta=\delta$. (b) Long-range mass relocation and island area reduction at low humidity. Light grey layers represent a G2–G3 arrangement while dark grey layers are G1–$SO_4$.

Fig. 9(a) for a total charge neutralization $\delta-=\delta+$ in the island cliff area.

The growth of the second layer provides a base for the linkage of original round islands. This is evidenced in Fig. 4 for some "8" shaped structures (*i.e.*, two neighboring islands) which already have a common second layer. On the basis of observed surface topographies, the connection process of two separate islands is schematically illustrated in Fig. 9(a).

### Localized mass movements in a negative domain

The growth of the second layer in islands needs a nutrient supply and this is achieved with molecular relocation from the same surface. At constant temperature and humidity of RH = 70%, as in the cases shown in Fig. 4, and many hours after the cleavage, the liquid film above the crystal surface is now saturated with the solute molecules, *i.e.*, at low under-saturation.[28] Therefore, the growth of the second layer can be attributed to mass movement of glycinium ions and sulfate ions from the adjacent area. This is evidenced by the simultaneous enlargement of the holes next to the islands, as shown in Fig. 4. In such a case, water molecules in the liquid film play simply the role of carrier to transport materials from the neighboring holes to the growing islands.

Apart from the above mass movement, another type of localized mass transport which can be recognized is the direct crystallization of TGS molecules from the saturated liquid film when the humidity is lowered. Upon dehumidification (*i.e.*, with the loss of water molecules from the liquid film), liquid phase TGS molecules are forced to crystallize onto some low-coordinated sites (or high surface energy sites), such as the walls of the holes and islands. This direct crystallization is shown in Fig. 5. The holes created at high humidity (RH = 70%) are now completely filled up in Fig. 5(c). Island pairing, island enlargement, and "island-on-island" growth, as described in the Results section, are also observed upon dehumidification or direct crystallization.

### Long range mass relocation in a negative domain

The above two types of mass movement occur at relatively localized areas, such as from the adjacent holes to the neighboring islands and from the liquid film to the solid surfaces immediately below. At constant low humidity, however, long range mass relocation takes place with longer experimental times, as shown in Fig. 6. The decrease in island density over time can be attributed to the minimization of the total energy of the crystal surface that includes surface energy of island walls (or boundary length for simplicity) and potential energy (in a gravitational field) of TGS molecules in the islands. It should be mentioned that the gravitational effect on the system energy is small or negligible because the height difference between the TGS layers is small. Surface structures depicted at the top of Fig. 9(b) are observed on the negative domain end. Apparently, the process suggested in Fig. 9(b) is in line with the total energy consideration, since it leads to flattened surfaces and reduces the total wall area of holes and islands. It should be mentioned that it is not possible to monitor simultaneously the filling up process for the lower part of the crystal surface, due to a large separation from the area examined in Fig. 6. Nevertheless, it is valid to propose this long-range material relocation model, in view of the direct observation of island density lowering (Fig. 6) and simple arguments based on energetic considerations and material balance principles.

The above long-range mass relocation can also be considered as surface recrystallization. As shown in the force images of Fig. 6, even under the low humidity conditions (RH = 51%), water molecules are still playing the role of carrier in transporting TGS molecules.

### Hole elimination and island isolation in a positive domain

Unlike a negative domain end (Figs. 4, 5, and 6), the material relocation on a positive domain end is less severe. In fact, drastic changes of surface topography only occur on dehumidification from RH = 70% to 57% (Figs. 2(b) to 7(a)). In the middle range of humidity (RH = 57–54%), as shown in Fig. 7, a noticeable change in surface topography is the reduction of hole number in both islands and flat crystal plane. At the lower end of this range (RH = 54%), only a subtle change of the surface can be recognized over a 6 h period, as can be seen in Fig. 8.

For the dehumidification from high humidity (Figs. 2(b) to 7(a)), both hole filling due to direct crystallization of liquid phase TGS to the solid phase and hole agglomeration can be ascribed to be the means for the hole elimination. In agreement with the direct crystallization model, total hole-area is reduced whereas island area is reduced only slightly. The agglomeration process, on the other hand, is revealed by the observation of hole-enlargement and a concurrent reduction of hole-number. In the cases of Fig. 7 at RH = 57–54%, hole agglomeration (rather than hole filling) is believed to be the main mechanism responsible for the hole-number reduction. This is also based on the observation that the area between the islands and holes (*i.e.*, the flat area) is increased, due to hole-agglomeration, and yet a constant total hole-area is maintained throughout the course of hole-agglomeration (from (a) to (d), Fig. 7). It should be noted that the islands on this domain end are distanced from the holes by the resulting flat zone. To further fill up the holes, TGS molecules of the islands have to cross over the flat zone. Since the size of islands reduces only slightly (almost unnoticeably), mass relocation of islands can be ignored. Again, this observation is in line with the hole-agglomeration mechanism.

A comparison of Fig. 8 ((a) to (d)) with Fig. 6 ((b) to (c)) indicates that the molecular mobility of TGS on the positive end is lower than that of the negative, although the humidity

for the cases in Fig. 8 is higher. The difference in mobility of TGS can be related to surface chemical composition and surface charge distribution, which is currently under investigation.

## Conclusions

In summary, time-resolved observations on water-assisted reconstruction of TGS have been made for two antiparallel ferroelectric domains with a humidity–temperature-controlled AFM. It is found that both holes and islands are present on the two types of domain ends at high humidity, due to a strong dissolution of TGS molecules. For a negative domain at constant high humidity, the observed island growth is at the expense of hole-enlargement. Upon dehumidification, the holes are filled up while the islands get larger and pair and/or link together. On prolonged standing at low humidity, islands on a negative domain reduce their sizes, owing to water-assisted molecular relocations. For a positive domain at high humidity, the holes can be formed inside an island. Upon dehumidification, the hole-number in a positive domain is reduced significantly, due to a direct crystallization and hole agglomeration process. The driving force of domain reconstruction can be related to molecular and crystal structures of TGS, mass transport in the surface region, and total energy lowering for the domain ends. Based on these results, reliable domain end assignment can be obtained by investigating surface topography at low humidity.

## Acknowledgements

The authors gratefully acknowledge the research funding (RP3960716) co-supported by the Ministry of Education and the National Science and Technology Board of Singapore. The authors thank Professor N. Nakatani of Toyama University, Japan, for providing the *b*-cut TGS crystals. S.B. also wishes to acknowledge postdoctoral fellowship awarded by the National Science and Technology Board of Singapore.

## References

1 E. A. Wood and A. M. Holden, *Acta. Crystallogr.*, 1957, **10**, 145.
2 S. Hoshino, Y. Okaya and R. Pepinski, *Phys. Rev.*, 1959, **115**, 323.
3 Y. Xu, *Ferroelectric Materials and Their Applications*, Elsevier Science, New York, 1991, ch. 7, pp. 286–292.
4 N. Nakatani, *Jpn. J. Appl. Phys.*, 1986, **25**, 27 and references therein.
5 N. Nakatani and M. Yoshio, *Jpn. J. Appl. Phys.*, 1996, **35**, L508.
6 N. Nakatani and M. Yoshio, *Jpn. J. Appl. Phys.*, 1996, **35**, 5752.
7 G. Ravi, S. Anbukumar, C. Subramanian, P. K. C. Pillai and P. Ramasamy, *Ferroelectrics*, 1995, **166**, 47.
8 O. W. Wang and C. S. Fang, *Cryst. Res. Technol.*, 1992, **27**, 245.
9 N. Nakatani, *J. Phys. Soc. Jpn.*, 1975, **39**, 741.
10 H. C. Zeng and S. K. Tung, *Chem. Mater.*, 1996, **8**, 2667.
11 H. C. Zeng, *J. Cryst. Growth*, 1997, **173**, 446.
12 H. C. Zeng, K. Tanaka, K. Hirao and N. Soga, *J. Non-Cryst. Solids*, 1997, **209**, 112.
13 S. Balakumar, J. B. Xu, J. X. Ma, S. Ganesamoorthy and I. H. Wilson, *Jpn. J. Appl. Phys.*, 1997, **36**, 5566.
14 S. Balakumar, J. B. Xu, I. H. Wilson, G. Arunmozhi, N. Nakatani and T. Yamazaki, *Jpn. J. Appl. Phys.*, 1997, **36**, 4377.
15 R. Luthi, H. Haefke, W. Gutmannsbauer, E. Meyer, L. Howald and H.-J. Guntherodt, *J. Vac. Sci. Technol. B*, 1994, **12**, 2451.
16 H. Haefke, R. Luthi, K.-P. Meyer and H.-J. Guntherodt, *Ferroelectrics*, 1994, **151**, 143.
17 J. Ohgami, Y. Sugawara, S. Morita, E. Nakamura and T. Ozaki, *Jpn. J. Appl. Phys.*, 1996, **35**, 2734.
18 J. Ohgami, Y. Sugawara, S. Morita, E. Nakamura and T. Ozaki, *Jpn. J. Appl. Phys.*, 1996, **35**, 5174.
19 A. Correia, J. Massanell, N. Garcia, A. P. Levanyuk, A. Zlatkin and J. Przeslawski, *Appl. Phys. Lett.*, 1996, **68**, 2796.
20 M.-K. Bae, K. Hara, S. Kai, H. Okabe and Y. Ishibashi, *Jpn. J. Appl. Phys.*, 1996, **65**, 2401.
21 H. Bluhm, R. Wiesendanger and K.-P. Meyer, *J. Vac. Sci. Technol. B*, 1996, **14**, 1180.
22 H. Bluhm, U. D. Schwarz, K.-P. Meyer and R. Wiesendanger, *Appl. Phys. A*, 1995, **61**, 525.
23 M.-K. Bae, T. Horiuchi, K. Hara, Y. Ishibashi and K. Matsushige, *Jpn. J. Appl. Phys.*, 1994, **33**, 1390.
24 K. Hara, M.-K. Bae, H. Okabe, T. Horiuchi, K. Matsushige and Y. Ishibashi, *Ferroelectrics*, 1995, **170**, 101.
25 A. M. Malyarevich and M. R. Posledovich, *J. Mol. Struct.*, 1996, **375**, 43.
26 S. R. Feletcher, E. T. Keve and A. C. Sakapski, *Ferroelectrics*, 1976, **14**, 775.
27 S. Balakumar and H. C. Zeng, in *Abstract Booklet, Innovations in Materials Conference*, ed. R. Roy, International Union of Materials Research Societies, Springer, Washington, D.C., 1998, p. 14.; *Mater. Res. Innovat.*, 1999, **2**, 289.
28 A. Sawada and R. Abe, *Jpn. J. Appl. Phys.*, 1967, **6**, 699.

*Paper a907937h*